

Stress and strain partition in elastic and plastic deformation of two phase alloys

THAK SANG BYUN, IN SUP KIM

Department of Nuclear Engineering, Korea Advanced Institute of Science and Technology,
PO Box 150 Cheongryang, Seoul 130-650, Korea

A stress and strain partition theory for two phase alloys was developed on the basis of the modified rules of mixtures. The extreme value condition of macroscopic strain energy density was found through Lagrangian multiplier method. Expressions for macroscopic elastic constants of two phase alloys were derived from the extreme value condition by assuming the strain linearity between constituent phases. Governing equation for stress and strain partition in plastic deformation was also obtained from the extreme value condition. The calculated elastic constants of WC-Co alloys fell invariably within the Hashin and Shtrikman's bounds. According to the governing equation the stress ratio between constituent phases was plotted as a function of strain increment ratio. By applying the governing equation to spheroidized carbon steel and duplex stainless steel, it was shown that the stress ratios, strain ratios, macroscopic stress-strain curves, and internal stresses could be evaluated from the *in situ* stress-strain curves of constituent phases.

1. Introduction

The stress and strain partition in two phase alloys results from the different mechanical properties between constituent phases [1–8]. Most of the elastic and plastic deformation behaviours of two phase alloys are related to the nonhomogeneous deformation. But there appears to be few general theories which can be applied to nonhomogeneous elastic and plastic deformation.

The elastic constants of two phase alloys vary nonlinearly with volume fractions. This phenomenon comes from the mutual interactions between the constituent phases whose elastic constants are different from each other. To predict elastic constants of composite body, extreme value theories have been frequently applied. Paul [9] derived lower and upper bounds of macroscopic elastic constants from the energy theorems, and Hashin and Shtrikman [10, 11] found other bounds from the variational principles. The results were in good agreement with the experimental observations [12–16] and with the finite element methods [17], but the theories could not describe the plastic deformation behaviours.

During plastic deformation of two phase alloys the plastic incompatibility between constituent phases causes the internal stress. It was known that plastic relaxation starts to occur after about 1 per cent strain [18–20]. But the internal stress from the unrelaxed plastic incompatibility plays an important role in stress and strain partition. If the *in situ* stress-strain curves of constituent phases are known, which could be obtained by the dislocation density models [1, 8, 18, 19], estimation of the internal stress is a major procedure on the calculation of the stress and strain partition. The internal stress has been evaluated by

several theoretical approaches: the continuum theories [7, 21–25], the shear-lag models [26, 27] and the dislocation continuum theory [20], and by experimental methods: the Bauschinger effect test [8, 30] and the X-ray diffraction test [29]. The present theory will supply a method by which the partitioned stresses and strains and the internal stresses can be directly calculated from the *in situ* flow curves of constituent phases.

The objectives of the present paper are to develop a general theory for elastically or plastically nonhomogeneous deformation, and to demonstrate the validity of the theory by applications to practical alloys. In the following sections, it is assumed that strain energy density has an extremum during deformation to develop a new stress and strain partition theory. The extreme value condition was derived through the Lagrangian multiplier method [34], and was used to obtain the equations for elastic constants and the governing equation for stress and strain partition of two phase alloys. The newly developed theory was tested by application to representative cases: macroscopic elastic constants of WC-Co alloys, stress and strain partition of a duplex stainless steel and of a spheroidized carbon steel.

2. Stress and strain partition theory

The modified rule of mixtures was suggested by Tamura *et al.* [33]. It was shown that macroscopic stress and strain can be adequately calculated from the *in situ* stress and strain of each constituent phase by the modified rule of mixtures [1]. Recently, Cho and Gurland [8] derived the modified rule of mixtures for two phase alloys by a stereological approach. The

modified rules of mixtures for ij -component of stress and strain in cartesian coordinates can be written by

$$\sigma_{ij} = f_1 \sigma_{ij}^1 + f_2 \sigma_{ij}^2 \quad (1)$$

$$\varepsilon_{ij} = f_1 \varepsilon_{ij}^1 + f_2 \varepsilon_{ij}^2 \quad (2)$$

where σ_{ij} and ε_{ij} are macroscopic stress and strain while σ_{ij}^1 , σ_{ij}^2 , ε_{ij}^1 , and ε_{ij}^2 are *in situ* average stresses and average strains in phase 1 and phase 2, and f_1 and f_2 are the volume fractions.

The macroscopic strain energy density U can be expressed by

$$U = \int \sigma_{ij} d\varepsilon_{ij} \quad (3)$$

where the summation convention for tensor component was used. Differentiating Equation 2,

$$d\varepsilon_{ij} = f_1 d\varepsilon_{ij}^1 + f_2 d\varepsilon_{ij}^2 \quad (4)$$

then macroscopic strain energy density of Equation 3 becomes

$$U = f_1^2 \int \sigma_{ij}^1 d\varepsilon_{ij}^1 + f_1 f_2 [\int \sigma_{ij}^1 d\varepsilon_{ij}^2 + \int \sigma_{ij}^2 d\varepsilon_{ij}^1] + f_2^2 \int \sigma_{ij}^2 d\varepsilon_{ij}^2 \quad (5)$$

This macroscopic strain energy density increases with increasing ε_{ij}^1 and ε_{ij}^2 . But the increasing path of the strain energy density is constrained by the microstructure of specimen and the loading conditions. Generally, the constraints give the minimized or maximized path, along which energy of the system increases. Thus we shall assume that macroscopic strain energy density U has an extreme value during deformation.

Lagrangian multiplier method [34] is used to find the extreme value condition. In this method the constraints are incorporated into the increment of physical quantity by means of multipliers. In the deformation of two phase alloys various constraints can be formulated from the microstructural properties; namely, shape, alignment and volume fractions of constituent phases, and from the loading mode. Here one constraint for volume fractions is used to derive a general extreme value condition of strain energy density.

The constraint for volume fractions is

$$C = f_1 + f_2 - 1 = 0 \quad (6)$$

One can regard the strains of each phase as constant values for the theory development. Differentiating U and C by f_1 and f_2 gives

$$dU = \frac{\partial U}{\partial f_1} df_1 + \frac{\partial U}{\partial f_2} df_2 \quad (7)$$

and

$$dC = \frac{\partial C}{\partial f_1} df_1 + \frac{\partial C}{\partial f_2} df_2 \quad (8)$$

Lagrangian multiplier λ is introduced to construct the extreme value condition of U such as [34]

$$dU + \lambda dC = 0 \quad (9)$$

Inserting Equations 7 and 8 into Equation 9, then we obtain

$$\frac{\partial U}{\partial f_1} + \lambda \frac{\partial C}{\partial f_1} = 0 \quad (10)$$

$$\frac{\partial U}{\partial f_2} + \lambda \frac{\partial C}{\partial f_2} = 0 \quad (11)$$

Since Equation 6 gives the following condition,

$$\frac{\partial C}{\partial f_1} = \frac{\partial C}{\partial f_2} = 1 \quad (12)$$

one can write

$$\frac{\partial U}{\partial f_1} = \frac{\partial U}{\partial f_2} = -\lambda \quad (13)$$

where λ is a constant which need not be determined. When this condition is satisfied, U is an extremum at a stress-strain state.

Inserting Equation 5 into Equation (13),

$$2f_1 \int \sigma_{ij}^1 d\varepsilon_{ij}^1 + f_2 \int \sigma_{ij}^1 d\varepsilon_{ij}^2 + f_2 \int \sigma_{ij}^2 d\varepsilon_{ij}^1 = 2f_2 \int \sigma_{ij}^2 d\varepsilon_{ij}^2 + f_1 \int \sigma_{ij}^1 d\varepsilon_{ij}^2 + f_1 \int \sigma_{ij}^2 d\varepsilon_{ij}^1 \quad (14)$$

Removing the integral notation,

$$[\sigma_{ij}^2 - \sigma_{ij}^1][(1-f)d\varepsilon_{ij}^1 + f d\varepsilon_{ij}^2] + [(1-f)\sigma_{ij}^1 + f\sigma_{ij}^2][d\varepsilon_{ij}^2 - d\varepsilon_{ij}^1] = 0 \quad (15)$$

where $f_1 = 1 - f$ and $f_2 = f$. With the modified rules of mixtures, Equations 1 and 2, the above equation becomes

$$(\sigma_{ij}^2 - \sigma_{ij}^1)d\varepsilon_{ij} + \sigma_{ij}(d\varepsilon_{ij}^2 - d\varepsilon_{ij}^1) = 0 \quad (16)$$

One can regard Equation 16 (or Equation 15) as a general governing equation for nonhomogeneous elastic and plastic deformation. In the later sections Equations 15 and 16 will be used to derive expressions for the macroscopic elastic constants and the governing equation for stress and strain partition in the plastic deformation of two phase alloys.

On the other hand Equation 15 can be also obtained by applying the following equation to Equation 5,

$$\frac{dU}{df} = 0 \quad (17)$$

This equation indicates that U has the extreme value when it is satisfied with Equation 13. Generally, the soft phase in the two phase alloys deforms more rapidly than the hard phase, so that the strain increment of the soft phase is larger than that of the hard phase. But the hard phase receives higher stress than the soft phase because load transfer occurs from the soft phase to the hard phase [8, 27]. Therefore assuming phase 2 is the harder phase, the conditions that $\sigma_{ij}^1 < \sigma_{ij}^2$ and $d\varepsilon_{ij}^1 > d\varepsilon_{ij}^2$ are obtained. Thus the second order derivative of U (see Equation 5) satisfies

$$\frac{d^2U}{df^2} = 2 \int (\sigma_{ij}^1 - \sigma_{ij}^2)(d\varepsilon_{ij}^1 - d\varepsilon_{ij}^2) < 0 \quad (18)$$

Hence it appears that U increases along the maximized path on straining.

3. Macroscopic elastic constants

In this section the methods to derive the expressions for elastic constants of the isotropic composite from

Equation 15 are suggested. For simplicity, the microstructure of the composite body is assumed such that equiaxed second phase particles are uniformly embedded in matrix. It is also assumed that constituent phases are elastically isotropic. With these conditions the composite is also elastically isotropic. When a material is elastically isotropic, all elastic constants are to be calculated from two known elastic constants by the correlations between the elastic constants. Thus the expressions for shear modulus G and for bulk modulus K are firstly obtained from Equation 15.

3.1. Shear modulus G

Assuming that two phase body is subjected to external shear stress along the 12-direction, and the stress is within elastic limit, then the 12 and 21-components of macroscopic stress and strain can exist (see Equation 16). And the 12 and 21-components of stress and strain are the same as each other at individual phases and at the composite of the phases. Therefore Equation 15 becomes

$$2[\sigma_{12}^2 - \sigma_{12}^1][(1-f)d\varepsilon_{12}^1 + f d\varepsilon_{12}^2] + 2[(1-f)\sigma_{12}^1 + f\sigma_{12}^2][d\varepsilon_{12}^2 - d\varepsilon_{12}^1] = 0 \quad (19)$$

Shear stress ratio between phase 1 and phase 2 is obtained from Equation 19, thus

$$\frac{\sigma_{12}^2}{\sigma_{12}^1} = \frac{2(1-f) + (2f-1)(d\varepsilon_{12}^2/d\varepsilon_{12}^1)}{(1-2f) + 2f(d\varepsilon_{12}^2/d\varepsilon_{12}^1)} \quad (20)$$

The constitutive equations between shear stress and elastic shear strain at respective phases are given by

$$\sigma_{12}^1 = 2G_1\varepsilon_{12}^1 \quad (21)$$

$$\sigma_{12}^2 = 2G_2\varepsilon_{12}^2 \quad (22)$$

where G_1 and G_2 are shear moduli of individual phases. It is assumed that the strain of one phase increases linearly with that of the other phase during elastic deformation. The linearity a_G for shear strains can be assumed as

$$\varepsilon_{12}^2 = a_G\varepsilon_{12}^1 \quad (23)$$

Then Equation 20 becomes

$$\frac{G_2}{G_1}a_G = \frac{2(1-f) + (2f-1)a_G}{(1-2f) + 2fa_G} \quad (24)$$

Rearranging the above equation,

$$\left(2f\frac{G_2}{G_1}\right)a_G^2 + \left(\frac{G_2}{G_1} + 1\right)(1-2f)a_G + 2(f-1) = 0 \quad (25)$$

If f , G_1 and G_2 are known by experiment, this second degree equation is easily solved for a_G .

The constitutive equation between σ_{12} and ε_{12} is given by

$$\sigma_{12} = 2G\varepsilon_{12} \quad (26)$$

Using the rules of mixtures Equation 1 and Equation 2, σ_{12} is given by σ_{12}^1 and σ_{12}^2 , and ε_{12} by ε_{12}^1 and ε_{12}^2 .

Thus macroscopic shear modulus of two phase body is

$$G = \frac{(1-f)\sigma_{12}^1 + f\sigma_{12}^2}{2[(1-f)\varepsilon_{12}^1 + f\varepsilon_{12}^2]} \quad (27)$$

Therefore, using Equations 21 to 23, the macroscopic shear modulus is represented as

$$G = \frac{(1-f)G_1 + fG_2a_G}{(1-f) + fa_G} \quad (28)$$

3.2. Bulk modulus K

When the two phase body is under hydrostatic stress, one can set

$$\sigma_{11} = \sigma_{22} = \sigma_{33} \quad (29)$$

$$\varepsilon_{11} = \varepsilon_{22} = \varepsilon_{33} \quad (30)$$

The stress and strain components of phase 1 and phase 2 are also satisfied with these two relations, and all the shear components are zero, then Equation 15 gives

$$3[\sigma_{11}^2 - \sigma_{11}^1][(1-f)d\varepsilon_{11}^1 + f d\varepsilon_{11}^2] + 3[(1-f)\sigma_{11}^1 + f\sigma_{11}^2][d\varepsilon_{11}^2 - d\varepsilon_{11}^1] = 0 \quad (31)$$

In a similar method to the shear modulus G , the bulk modulus K can be derived from hydrostatic stress ratio. The hydrostatic stress ratio between phase 1 and phase 2 is

$$\frac{\sigma_{11}^2}{\sigma_{11}^1} = \frac{2(1-f) + (2f-1)(d\varepsilon_{11}^2/d\varepsilon_{11}^1)}{(1-2f) + 2f(d\varepsilon_{11}^2/d\varepsilon_{11}^1)} \quad (32)$$

Noting that

$$\sigma_{11}^1 = 3K_1\varepsilon_{11}^1 \quad (33)$$

$$\sigma_{11}^2 = 3K_2\varepsilon_{11}^2 \quad (34)$$

where K_1 and K_2 are the bulk moduli of respective phases. And if the linearity a_K between ε_{11}^1 and ε_{11}^2 is assumed such that

$$\varepsilon_{11}^2 = a_K\varepsilon_{11}^1 \quad (35)$$

Then, Equation 32 becomes

$$\left(2f\frac{K_2}{K_1}\right)a_K^2 + \left(\frac{K_2}{K_1} + 1\right) \times (1-2f)a_K + 2(f-1) = 0 \quad (36)$$

where a_K can be obtained.

On the other hand, macroscopic bulk modulus K is given by

$$\sigma_{11} = 3K\varepsilon_{11} \quad (37)$$

Using the modified rules of mixtures Equations 1 and 2,

$$K = \frac{(1-f)\sigma_{11}^1 + f\sigma_{11}^2}{3[(1-f)\varepsilon_{11}^1 + f\varepsilon_{11}^2]} \quad (38)$$

By Equations 33 to 35 this becomes

$$K = \frac{(1-f)K_1 + fK_2a_K}{(1-f) + fa_K} \quad (39)$$

Other macroscopic elastic constants of Young's modulus E and Poisson's ratio ν are to be calculated from G and K that are already given at above derivation. The correlations between the elastic constants are given in the general elasticity theory.

4. Governing equation for stress and strain partition in the plastic deformation

The governing equation for the stress and strain partition during tensile deformation can also be derived from Equation 15. The stress component of individual phases is expressed by macroscopic stress and internal stress such as

$$\sigma_{ij}^1 = \sigma_{ij} + \sigma_{ij}^{1I} \quad (40)$$

$$\sigma_{ij}^2 = \sigma_{ij} + \sigma_{ij}^{2I} \quad (41)$$

where $1I$ and $2I$ denote internal stresses in phase 1 and 2. In the case that spherical or randomly oriented ellipsoidal second phase particles were embedded in matrix, and the composite body was under uniaxial load of tensile direction (11-direction), the relationships between internal stress components were derived to be [7, 29]

$$\sigma_{22}^{1I} = \sigma_{33}^{1I} = -\frac{1}{2}\sigma_{11}^{1I} \quad (42)$$

$$\sigma_{22}^{2I} = \sigma_{33}^{2I} = -\frac{1}{2}\sigma_{11}^{2I} \quad (43)$$

Furthermore the amount $(\sigma_{11}^2 - \sigma_{11}^1)$ in Equation 15 has been called the load transfer stress σ_{lr} . Since the load transfer stress have a relation with the internal stresses as

$$(\sigma_{11}^2 - \sigma_{11}^1) = (\sigma_{11}^{2I} - \sigma_{11}^{1I}) \quad (44)$$

one can derive the following relations

$$\begin{aligned} (\sigma_{22}^2 - \sigma_{22}^1) &= (\sigma_{22}^{2I} - \sigma_{22}^{1I}) \\ &= -\frac{1}{2}(\sigma_{11}^{2I} - \sigma_{11}^{1I}) = -\frac{1}{2}(\sigma_{11}^2 - \sigma_{11}^1) \end{aligned} \quad (45)$$

$$\begin{aligned} (\sigma_{33}^2 - \sigma_{33}^1) &= (\sigma_{33}^{2I} - \sigma_{33}^{1I}) \\ &= -\frac{1}{2}(\sigma_{11}^{2I} - \sigma_{11}^{1I}) = -\frac{1}{2}(\sigma_{11}^2 - \sigma_{11}^1) \end{aligned} \quad (46)$$

On the other hand, macroscopic plastic strains have the following relation [7]

$$\varepsilon_{22}^p = \varepsilon_{33}^p = -\frac{1}{2}\varepsilon_{11}^p \quad (47)$$

In the region of large plastic strain, we can assume that the total strains, elastic strains plus plastic strains, also satisfy the form of the above relations,

$$\varepsilon_{22} = \varepsilon_{33} \approx -\frac{1}{2}\varepsilon_{11} \quad (48)$$

The shear components of stresses and strains are zero. Using Equations 45 to 48, Equation 15 becomes

$$\begin{aligned} \frac{3}{2}[\sigma_{11}^2 - \sigma_{11}^1][(1-f)d\varepsilon_{11}^1 + f d\varepsilon_{11}^2] \\ + [(1-f)\sigma_{11}^1 + f\sigma_{11}^2][d\varepsilon_{11}^2 - d\varepsilon_{11}^1] = 0 \end{aligned} \quad (49)$$

Therefore, the governing equation for stress and strain partition in the plastic deformation of two phase alloys is given by

$$\frac{\sigma_{11}^2}{\sigma_{11}^1} = \frac{5(1-f) + (5f-2)(d\varepsilon_{11}^2/d\varepsilon_{11}^1)}{(3-5f) + 5f(d\varepsilon_{11}^2/d\varepsilon_{11}^1)} \quad (50)$$

It is noted that the stress ratio between constituent phases $(\sigma_{11}^2/\sigma_{11}^1)$ is represented as a function of the strain increment ratio $(d\varepsilon_{11}^2/d\varepsilon_{11}^1)$.

Using Equations 40 to 43, the equivalent stress of the phase 1 is derived to be

$$\begin{aligned} \sigma_{eq}^1 &= \frac{1}{\sqrt{2}}[(\sigma_{11}^1 - \sigma_{22}^1)^2 + (\sigma_{22}^1 - \sigma_{33}^1)^2 \\ &+ (\sigma_{33}^1 - \sigma_{11}^1)^2]^{1/2} = \sigma_{11} + \frac{3}{2}\sigma_{11}^{1I} \end{aligned} \quad (51)$$

likewise that of the phase 2 is

$$\sigma_{eq}^2 = \sigma_{11} + \frac{3}{2}\sigma_{11}^{2I} \quad (52)$$

In the case that plastic strain is dominant at both phases, it is possible that

$$\varepsilon_{eq}^{1p} = \varepsilon_{11}^{1p} \approx \varepsilon_{11}^1 \quad (53)$$

$$\varepsilon_{eq}^{2p} = \varepsilon_{11}^{2p} \approx \varepsilon_{11}^2 \quad (54)$$

where ε_{eq}^{1p} and ε_{eq}^{2p} are the equivalent plastic strains of phase 1 and 2. Then the ratio between the equivalent stresses of constituent phases can be obtained from Equation 49,

$$\frac{\sigma_{eq}^2}{\sigma_{eq}^1} = \frac{2(1-f) + (2f-1)(d\varepsilon_{eq}^{2p}/d\varepsilon_{eq}^{1p})}{(1-2f) + 2f(d\varepsilon_{eq}^{2p}/d\varepsilon_{eq}^{1p})} \quad (55)$$

5. Applications and discussions

5.1. Macroscopic elastic constants of tungsten carbide-cobalt (WC-Co) alloys

In this section the theoretical analysis for various elastic constants will be verified by comparison with other theoretical approaches. The WC-Co composites have been frequently studied in terms of the relations between macroscopic elastic constants and volume fraction of constituent phases. Various volume fractions of WC in WC-Co alloys are easily obtained by sintering of the mixture of WC and Co powders, and there is large difference between the elastic constants of WC and Co. The cobalt is softer than the tungsten-carbide, thus the cobalt was regarded as the phase 1 and the tungsten-carbide the phase 2 (hard phase). According to the literature [9, 16] the elastic constants of $G_1 = 80.2$ and $K_1 = 184.2$ for Co and $G_2 = 293.1$ and $K_2 = 381.3$ for WC were used for theoretical calculation of the elastic constants of the composites. The exact solutions for macroscopic shear modulus G and bulk modulus K can be given by means of Equation 28 and Equation 39. Thus the values of G and K have to be firstly determined. The other macroscopic elastic constants such as Young's modulus E and Poisson's ratio ν were calculated from the values of G and K .

The elastic strain linearity a_G was estimated by inserting shear moduli of WC and Co into Equation 25. Then, the macroscopic shear modulus G was calculated from the a_G values. Likewise the elastic strain linearity a_K under hydrostatic stress was calculated from Equation 36, and the calculated values were used to evaluate K . The calculated values of a_G and a_K are shown in Table I. Both a_G and a_K increase with volume fraction of WC. And the a_G value is lower than a_K value, which seems to be caused by the greater

TABLE I The calculated values of macroscopic elastic constants of WC-Co alloys. Strain linearities a_G and a_K are listed with volume fraction of WC. The upper and lower bounds were calculated from Hashin and Shtrikman's equations [11].

f(WC)	a_G	a_K		G(GPa)	K(GPa)	E(GPa)	ν
0.0	0.4296	0.6515	Co	80.2	184.2	210.0	0.3100
0.1	0.4444	0.6596	Upper Bound	94.2	199.3	244.1	0.3010
			Theory	90.2	197.7	234.8	0.3009
			Lower Bound	90.1	196.5	234.6	0.2958
0.2	0.4612	0.6681	Upper Bound	109.4	215.1	280.6	0.2919
			Theory	102.2	212.4	264.2	0.2917
			Lower Bound	101.4	209.8	261.9	0.2827
0.3	0.4801	0.6768	Upper Bound	125.8	231.9	319.5	0.2825
			Theory	116.5	228.5	298.7	0.2821
			Lower Bound	114.1	224.3	292.7	0.2704
0.4	0.5007	0.6859	Upper Bound	143.6	249.6	361.4	0.2727
			Theory	133.5	246.0	339.1	0.2703
			Lower Bound	128.7	240.3	327.6	0.2587
0.5	0.5229	0.6951	Upper Bound	162.9	268.3	406.5	0.2625
			Theory	153.3	265.0	385.5	0.2575
			Lower Bound	145.5	257.8	367.4	0.2475
0.6	0.5461	0.7044	Upper Bound	184.1	288.2	455.4	0.2515
			Theory	176.1	285.5	438.1	0.2442
			Lower Bound	165.2	277.2	413.4	0.2366
0.7	0.5696	0.7138	Upper Bound	207.4	309.3	508.5	0.2395
			Theory	201.7	307.3	496.5	0.2308
			Lower Bound	188.4	298.9	467.0	0.2260
0.8	0.5928	0.7232	Upper Bound	233.0	331.7	566.4	0.2263
			Theory	230.0	330.6	560.0	0.2177
			Lower Bound	216.3	323.1	530.5	0.2154
0.9	0.6153	0.7325	Upper Bound	261.5	355.7	630.0	0.2114
			Theory	260.6	355.3	628.1	0.2054
			Lower Bound	250.4	350.5	606.7	0.2048
1.0	0.6367	0.7416	WC	293.1	381.3	700.0	0.1940

value of G_2/G_1 ($= 3.66$) than the value of K_2/K_1 ($= 2.07$). It is worth to note that a_G and a_K are always less than 1.0 for all alloys which are satisfied with the conditions that $G_2 > G_1$ and $K_2 > K_1$. Paul [9] showed that the iso-strain theory gave the upper bounds of elastic moduli and the iso-stress theory the lower bounds. Since $a_G = 1.0$ or $a_K = 1.0$ means the validity of the iso-strain theory, it is evident that the macroscopic moduli by the present theory are under the Paul's upper bounds.

The calculated values of G , K , E and ν were compared with the Hashin and Shtrikman's bounds [10, 11] in Table I. The various elastic moduli of WC-Co composites estimated by experiments [12–16] depended solely on the volume fraction of WC, and they fell within the Hashin and Shtrikman's bounds. The elastic constants calculated by the present theory also invariably fall between the Hashin and Shtrikman's bounds, hence it is evident that the present theory can well describe the elastic deformation of two phase alloys.

5.2. General aspects of the governing equation for stress and strain partition in the plastic deformation of two phase alloys

To solve the governing equation (Equation 50) one must know the *in situ* constitutive equations of

σ_{11}^1 versus ϵ_{11}^1 and σ_{11}^2 versus ϵ_{11}^2 . In plastic region Hollomon equation or Ludwick equation may be useful to obtain *in situ* flow curves of the constituent phases. The *in situ* flow curve is the stress-strain relation when the constituent phases constrain each other in the phase aggregate, and is different from the flow curve of a free single phase. Estimation of the *in situ* flow curve is not the scope of the present paper, so that the reported data would be used for calculations in the following sections.

Equation 50 can be rewritten as

$$\frac{\sigma_2}{\sigma_1} = \frac{5(1-f) + (5f-2)(d\epsilon_2/d\epsilon_1)}{(3-5f) + 5f(d\epsilon_2/d\epsilon_1)} \quad (56)$$

where subscripts 1 and 2 mean the phase 1 and 2, and all stresses and strains are 11-components. According to this equation stress ratio (σ_2/σ_1) was plotted in Fig. 1 as a function of strain increment ratio ($d\epsilon_2/d\epsilon_1$) for several hard phase volume fraction f . The following facts were revealed by inspection of the Fig. 1: 1. The solution curve can be interpreted such that a deformation state corresponds to a point ($\sigma_2/\sigma_1, d\epsilon_2/d\epsilon_1$) on the curve of given f ; 2. All of the solution curves have a trend to decrease with increase of strain increment ratio. This means that the material whose constituent phases have small strength difference, and give large values of $d\epsilon_2/d\epsilon_1$ reveals small stress concentration on hard phase; 3. Position of

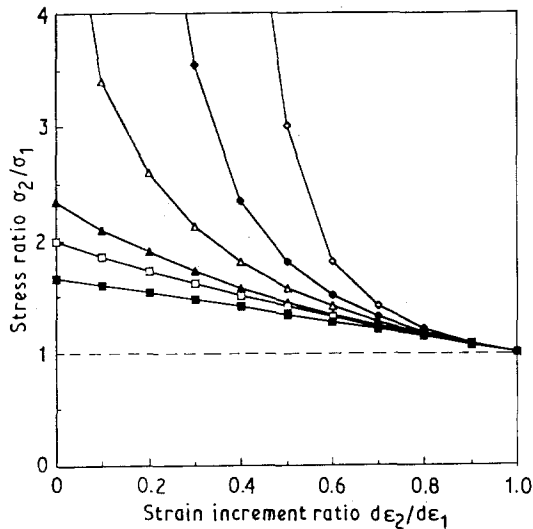


Figure 1 Stress ratio σ_2/σ_1 as a function of strain increment ratio $d\epsilon_2/d\epsilon_1$ for several volume fraction of hard phase (phase 2), f : (\diamond) 1.0, (\blacklozenge) 0.7, (\triangle) 0.5, (\blacktriangle) 0.3, (\square) 0.2 and (\blacksquare) 0.0.

solution curve moves up with increase of volume fraction of hard phase f . This illustrates that the intensity of stress concentration on hard phase can increase as f increases. Resultantly, high stress concentration may derive early initiation of plastic deformation of the hard phase although deformation of the soft phase proceeds in a more rapid rate; 4. The solution curves in Fig. 1 fall between the iso-stress line ($\sigma_2/\sigma_1 = 1.0$) and the iso-strain line ($d\epsilon_2/d\epsilon_1 = 1.0$); 5. The solution curves converge to the point that σ_2/σ_1 and $d\epsilon_2/d\epsilon_1$ are simultaneously equal to unity. This means that if two phase alloy is subjected to the iso-stress condition, it must be also subjected to the iso-strain condition. This phenomenon may occur if the flow curve of one phase is the same as that of the other. Therefore it can be said that the composite with low strength difference between constituent phases reveals relatively homogeneous strain distribution during deformation.

5.3. Calculation of stress and strain partition in spheroidized carbon steel and duplex stainless steel

Two phase alloys are sometimes classified into two groups [2, 8]. Alloys which belong to the first group are composed of soft matrix and a small amount of high strength second phase such as spheroidized carbon steels [8, 25, 29–31] or dual phase steels [2, 3, 28], in which the matrix deforms plastically but the second phase particles elastically in most uniform strain range. Alloys in the second group consist of matrix and a large amount of easily deformable second phase. Alloys such as duplex stainless steels [8] or low carbon dual phase steels [2, 4] belong to this group. Harder phase in the second group of alloys undergoes plastic deformation at a small strain. Therefore two representative two phase alloys, i.e., a spheroidized carbon steel [29] in the first alloy group and a duplex stainless steel [8] in the second alloy group, were adopted to demonstrate the applicability of the pres-

ent theory. And the partition of stress and strain during plastic deformation was calculated by using Equation 56.

The spheroidized carbon steel [29] contains 1.14 wt % carbon and 17 per cent cementite. Ferrite (α) and cementite (β) are denoted by, respectively, phase 1 (soft phase) and phase 2 (hard phase) in the steel. The stresses at ferrite (σ_1) were evaluated from the residual internal stress data which were calculated from the X-ray diffractions [29] by using the following equation

$$\sigma_1 = \sigma + \sigma_1^{RI} \quad (57)$$

where σ is the macroscopic stress, and σ_1^{RI} is the residual internal stress in the ferrite matrix. And the strains at ferrite (ϵ_1) were given by

$$\epsilon_1 = \frac{\epsilon_p}{1-f} + \frac{\sigma_1}{E} \quad (58)$$

where ϵ_p is the macroscopic plastic strain, the first term is the plastic strain of the ferrite when the cementite have no plasticity, and the second term is the elastic strain ($E = 207$ GPa). Then the *in situ* flow curve of ferrite matrix was fitted to be $\sigma_1 = 1022\epsilon_1^{0.164}$ (MPa). The constitutive equation for cementite (Fe_3C) was given by $\sigma_2 = 180\epsilon_2$ (GPa) [35].

On the other hand, the duplex stainless steel [8] includes 40 per cent austenite (γ) and 60 per cent ferrite (α). Two hollomon curves, which were fitted from the data in the literature [8], were $\sigma_1 = 1020\epsilon_1^{0.1}$ for γ phase and $\sigma_2 = 1025\epsilon_2^{0.043}$ for α phase. The Young's modulus of ferrite and austenite contained in above steels was 207 GPa.

Introducing the *in situ* stress-strain curves into the governing equation, Equation 56, then the equation had only two unknowns ϵ_1 and ϵ_2 . ϵ_1 was assumed firstly and ϵ_2 was found by a computer program containing the bisection method. Then macroscopic stresses and strains were calculated from the partitioned stresses and strains. Internal stresses were also calculated by using Equations 40 and 41.

Fig. 2 shows the relation between the stress-strain curves of *in situ* ferrite, cementite and their composite. The flow curve of the composite (spheroidized carbon steel) is similar with the experimental curve [29]. The dashed tie lines, connecting the corresponding partitioned stresses and strains of ferrite and cementite, are marked at several macroscopic strains 0.01, 0.03, 0.05 and 0.07.

Fig. 3 also shows the stress-strain curves of *in situ* austenite, ferrite and their composite. The flow curve of the composite (duplex stainless steel) is compared with the experimental curve [8]. The dashed tie lines are also marked at macroscopic strains 0.01, 0.03, 0.05 and 0.07. Comparing Fig. 2 with Fig. 3, one can recognize that degree of stress and strain partition is much more severe in spheroidized carbon steel than in duplex stainless steel. This difference seems to be because there is a large strength difference between the hard phases such as the cementite in spheroidized carbon steel and the ferrite in duplex stainless steel.

Fig. 4 represents variations of stress ratio (σ_2/σ_1) which come from Fig. 2 and Fig. 3. The stress ratio in

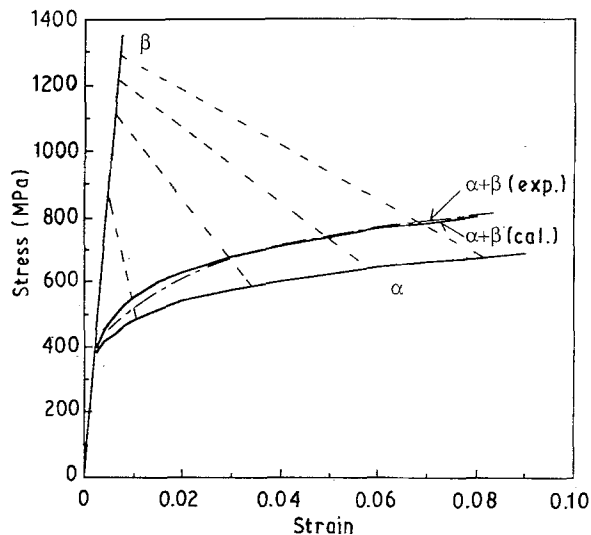


Figure 2 The calculated stress-strain curve of spheroidized carbon steel ($\alpha + \beta$) and the *in situ* stress-strain curves of ferrite (α) and cementite (β). The tie lines connecting the three stress-strain curves are indicated at $\epsilon = 0.01, 0.03, 0.05$ and 0.07 . The experimental stress-strain curve [29] is compared with the calculated curve.

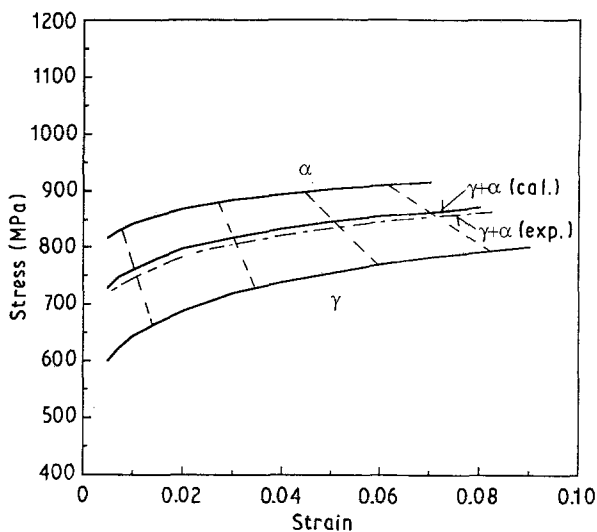


Figure 3 The calculated stress-strain curve of duplex stainless steel ($\gamma + \alpha$) and the *in situ* stress-strain curves of austenite (γ) and ferrite (α). The tie lines connecting the three stress-strain curves are indicated at $\epsilon = 0.01, 0.03, 0.05$ and 0.07 . The experimental stress-strain curve [8] is compared with the calculated curve.

the spheroidized carbon steel increases rapidly up to about 1.9 and is saturated at $\epsilon \approx 0.02$. The stress ratio in the dual phase steel composed of about 15 per cent martensite and ferrite matrix was estimated to be 2.24 by the shear-lag theory [28]. And Cho and Gurland [8] showed that the value was 1.5–1.6 after saturation for a spheroidized carbon steel, in which volume fraction of cementite was 0.167. Hence it can be concluded that the present theory gives reasonable values of the stress ratios.

The stress ratio in the duplex stainless steel decreases from about 1.35 as seen in Fig. 4. Since the stress ratio within elastic limit of both constituent phases is 1.0, this is because the Young's moduli of the two constituent phases was assumed to be equal, the value might be rapidly increased from 1.0 up to 1.35 at

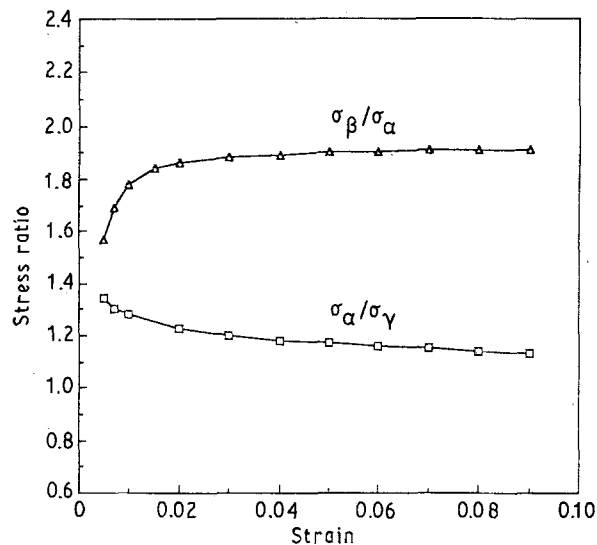


Figure 4 Stress ratio as a function of strain for (Δ) spheroidized carbon steel ($\alpha + \beta$) and (\square) duplex stainless steel ($\gamma + \alpha$).

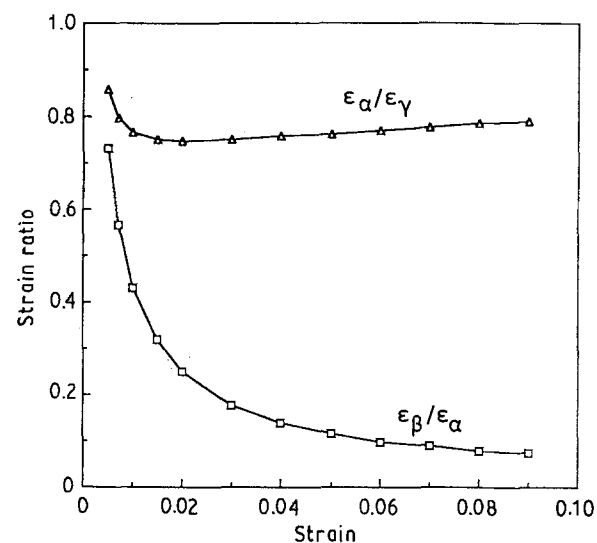


Figure 5 Strain ratio as a function of strain for (\square) spheroidized carbon steel ($\alpha + \beta$) and (Δ) duplex stainless steel ($\gamma + \alpha$).

initial straining ($0.0 < \epsilon < 0.005$). Cho and Gurland [8] showed that the stress ratio of this steel was a constant value of about 1.17 after $\epsilon = 0.02$. This value agrees well with the value of the present calculation. In spite of large amount of ferrite (hard phase; $f = 0.6$) the stress ratio in the duplex stainless steel is less than that in the spheroidized carbon steel. This seems because of early relaxation of stress concentration by easy deformation of ferrite.

The strain ratio (ϵ_2/ϵ_1) for the two alloys are shown in Fig. 5. The strain ratio of the spheroidized carbon steel rapidly decreases to go below 0.1 with strain, while that of the duplex stainless steel decreases to a minimum point and increases slightly from the point with subsequent increase of strain. Cho and Gurland [8] measured the phase strains by means of the microgrid mesh imprinted by photolithography. For example, they showed that the strain ratio of the duplex stainless steel was 0.77 at $\epsilon = 0.06$, and that of a spheroidized carbon steel 0.066 at $\epsilon = 0.05$. It can be

noted that strain ratio is very sensitive to strength difference between constituent phases and to volume fractions [2].

5.4. Internal stress by nonhomogeneous deformation

The internal stress of tensile direction (11-direction) was estimated from the partitioned stresses of respective phases and the macroscopic flow stress by means of Equations 40 and 41. Fig. 6 shows the internal stress variation of spheroidized carbon steel. Internal stress of matrix σ_{11}^I , which is equal to $(-)\sigma_B$ (back stress), is balanced with that of second phase σ_{11}^{II} . Hence the signs of those are opposite each other. It can be noted that the absolute value of the internal stress has a similar trend to the stress ratio. The internal stresses (absolute values) of both phases increase rapidly at initial straining.

Using the Eshelby's solution for inclusion transformation [21, 22], several continuum models [7, 23–25] and dislocation continuum model [20] have been developed to estimate internal stress. Recently, Chang and Asaro [31] used a continuum model to estimate the internal stress of the ferrite matrix of spheroidized carbon steels. In their model the result of the continuum theories [20–22] was modified by Bauschinger effect test data, namely, permanent softening stresses. They showed that in spheroidized carbon steel the internal stress generated by unrelaxed plastic incompatibility saturates at 3–5 per cent strain. It was found that internal stress contributes about 20 per cent of the total strain hardening.

Wilson and Konnan [29] measured the residual internal stress of spheroidized carbon steel after unloading by using the X-ray diffraction method. In small strain range the residual internal stresses measured by X-ray diffraction were smaller than the *in situ* internal stresses given by the present calculation. This may be because at small strains X-ray measurements

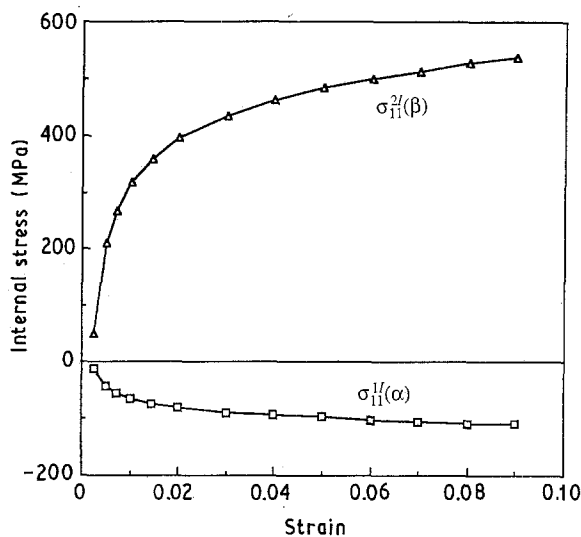


Figure 6 Internal stress development in spheroidized carbon steel ($\alpha + \beta$) on straining. Tensile components (11-components) are shown. The internal stress of ferrite (α) is balanced with that of cementite (β); $(1 - f)\sigma_{11}^I(\alpha) + f\sigma_{11}^{II}(\beta) = 0$, ($f = 0.17$).

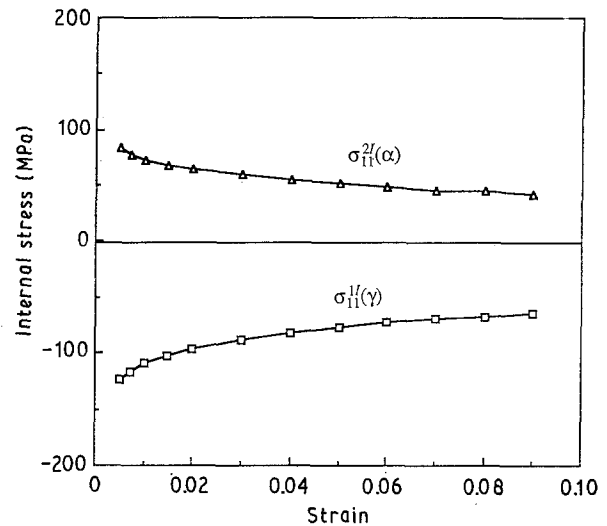


Figure 7 Internal stress development in duplex stainless steel ($\gamma + \alpha$) on straining. Tensile components (11-components) are shown. The internal stress of austenite (γ) is balanced with that of ferrite (α); $(1 - f)\sigma_{11}^I(\gamma) + f\sigma_{11}^{II}(\alpha) = 0$, ($f = 0.60$).

are largely subjected to general relaxation during unloading, and subjected to local relaxation at X-ray diffracting subsurface layer [32]. But in large strain range the calculated values of $\sigma_{11}^I(\alpha)$ (Fig. 6) agree well with the residual internal stress data [29]; for example, both the X-ray measurement and the present calculation gave about 107 MPa at 7% strain.

Bauschinger effect test has been frequently conducted to obtain internal stress [8, 30]. The internal stress in matrix (σ_{IX}) measured by X-ray diffraction and the permanent softening stress (σ_{ps}) in reversed loading have a relationship that $\sigma_{IX} \approx 0.5\sigma_{ps}$ [30, 32]. But this relationship can not be applied to duplex alloys. Cho and Gurland [8] used a special method to obtain back stress from the transient softening in reversed straining. This was because no permanent softening was observed in Bauschinger test for α - γ duplex stainless steel. If flow resistance is caused by weak obstacles which are permeable to dislocations, then the lowering of flow stress in reversed straining will be only a transient effect [32]. Thus the Bauschinger effect test seems unsuitable for determination of the *in situ* internal stresses of duplex alloys. But the present theory might supply a useful tool for estimation of the *in situ* internal stress development during deformation. The internal stresses of duplex stainless steel is successfully evaluated by the present theory, and they are illustrated in Fig. 7. The values in Fig. 7 have a good agreement with the reported data [8].

6. Conclusions

A new stress and strain partition theory for two phase alloys was developed. It was based on the assumption that macroscopic strain energy density had an extreme value during deformation. The Lagrangian multiplier method was used to find the extremum condition, from which the governing equation for non-homogeneous plastic deformation and the expressions for macroscopic elastic constants were obtained. The

following conclusions were drawn from inspection of the governing equation and from applications of the present theory to two phase alloys such as WC-Co alloys, a duplex stainless steel and a spheroidized carbon steel.

1. The formulas for macroscopic shear modulus G and macroscopic bulk modulus K could satisfactorily predict the G and K values of WC-Co alloys. Young's modulus E and Poisson's ratio ν were also calculated from the evaluated values of G and K . All the calculated elastic constants fell within the Hashin and Shtrikman's upper and lower bounds.

2. When the stress ratio was plotted as a function of the strain increment ratio according to the governing equation for nonhomogeneous plastic deformation, the plotted curves confirmed the well known facts that the stress ratio and strain ratio increase as the volume fraction of hard phase increases, and that large strength differences between constituent phases leads to high stress ratio and high strain hardening.

3. The fitted Hollomon equations of *in situ* individual phases and the bisection iterating method were used in the calculations of stress and strain partition. The calculated values of the stress ratio and strain ratio were in accordance with the reported data. The internal stresses and macroscopic stress-strain curves were also successfully estimated by the present theory.

References

1. H. FISCHMEISTER and B. KARLSSON, *Z. Metallkunde* **68** (1977) 311.
2. H. P. SHEN, T. C. LEI and J. Z. LIU, *Mat. Sci. and Tech.* **2** (1986) 28.
3. C. KIM, *Met. Trans.* **19A** (1988) 1263.
4. R. G. DAVIES, *ibid.* **9A** (1978) 451.
5. J. JINCH, S. ANKEM and H. MARGOLIN, *Mat. Sci. and Engng* **34** (1978) 203.
6. B. O. SUNDSTROM, *Mat. Sci. and Engng* **12** (1973) 265.
7. Y. TOMOTA, K. KUROKI, T. MORI and I. TAMURA, *Mat. Sci. and Engng* **24** (1976) 85.
8. K. CHO and J. GURLAND, *Met. Trans.* **19A** (1988) 2027.
9. B. PAUL, *Trans. TMS-AIME* **218** (1960) 36.
10. Z. HASHIN and S. SHTRIKMAN, *J. Appl. Mech. Trans. ASME* **29** (1962) 143.
11. Z. HASHIN and S. SHTRIKMAN, *J. Mech. Phys. Solids* **11** (1963) 127.
12. R. KIEFFER and P. SCHWARTZKOPF, in "Hartstoffe und Hartmetalle" (Springer, Vienna, 1953).
13. C. NISHIMATSU and J. GURLAND, *Trans. ASM* **52** (1960) 127.
14. E. LARDNER, *J. Inst. Met.* **80** (1951) 369.
15. F. F. VORONOV and D. B. BALASHOV, *Phys. Metals Metallog.* **2** (1960) 127.
16. H. DOI, Y. FUJIWARA, K. MIYAKE and Y. OOSAWA, *Met. Trans.* **1** (1970) 147.
17. B. O. JAENSSON and B. O. SUNDSTROM, *Mat. Sci. and Engng* **9** (1972) 217.
18. M. F. ASHBY, *Phil. Mag.* **14** (1966) 1157.
19. *Idem.*, *ibid.* **21** (1970) 399.
20. L. M. BROWN and W. M. STOBBS, *ibid.* **23** (1971) 1185.
21. J. D. ESHELBY, *Proc. Roy. Soc. A* **241** (1957) 241.
22. *Idem.*, *ibid.* **A252** (1959) 561.
23. K. TANAKA, T. MORI and T. NAKAMURA, *Phil. Mag.* **21** (1970) 267.
24. K. TANAKA and T. MORI, *Acta Metall.* **18** (1970) 931.
25. L. ANAND and J. GURLAND, *ibid.* **24** (1976) 901.
26. J. GURLAND, *Scripta Met.* **13** (1979) 967.
27. J. GURLAND, *Mat. Sci. and Engng* **40** (1979) 59.
28. A. F. SZEWCZYK and J. GURLAND, *Met. Trans.* **13A** (1982) 1821.
29. D. V. WILSON and Y. A. KONNAN, *Acta Metall.* **12** (1964) 617.
30. D. V. WILSON, *ibid.* **13** (1965) 807.
31. Y. W. CHANG and R. J. ASARO, *Mat. Sci.* **12** (1978) 277.
32. P. S. BATE and D. V. WILSON, *Acta Metall.* **34** (1986) 1097.
33. I. TAMURA, Y. TOMOTA and H. OZAWA, in Proceedings of the 3rd International Conference on Strength of Metals and Alloys, Institute of Metal and Iron and Steel Inst, London, Vol. 1 (1973) p. 611.
34. G. ARFKEN, in "Mathematical Methods for Physicists" (Academic Press, 2nd edn., 1982) p. 790.
35. L. A. GLIKMAN, A. M. KARTASHOV, Z. M. RUBASHKINA and A. F. FOBOV, *Problemy Prochnosti* **4** (1975) 123.

Received 12 June
and accepted 29 October 90